IN-64
136503
P.13

NASA Technical Memorandum 105928
ICOMP–92–21
CMOTT–92–10

Eno-Osher Schemes for Euler Equations

Jacobus J. Van Der Vegt
Institute for Computational Mechanics in Propulsion
Lewis Research Center
Cleveland, Ohio

and

Center for Turbulence Research
Stanford University
Stanford, California

November 1992

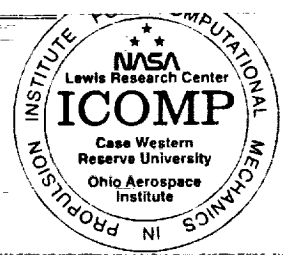

NASA

ENO-OSHER SCHEMES FOR EULER EQUATIONS

Jacobus J. Van Der Vegt

ICOMP/CMOTT NASA Lewis Research Center†
21000 Brookpark Road, Cleveland, OH 44135
and
Center for Turbulence Research, Stanford University,
Building 500, Stanford, CA94305

Abstract

In this paper the combination of the Osher approximate Riemann solver for the Euler equations and various ENO schemes is discussed for one-dimensional flow. The three basic approaches, viz. the ENO scheme using primitive variable reconstruction, either with the Cauchy-Kowalewski procedure for time integration or the TVD Runge-Kutta scheme, and the flux-ENO method are tested on different shock tube cases. The shock tube cases were chosen to present a serious challenge to the ENO schemes in order to test their ability to capture flow discontinuities, such as shocks. Also the effect of the ordering of the eigenvalues, viz. natural or reversed ordering, in the Osher scheme is investigated. The ENO schemes are tested up to fifth order accuracy in space and time. The ENO-Osher scheme using the Cauchy-Kowalewski procedure for time integration is found to be the most accurate and robust compared with the other methods and is also computationally efficient. The tests showed that the ENO schemes perform reasonably well, but have problems in cases where two discontinuites are close together. In that case there are not enough points in the smooth part of the flow to create a non-oscillatory interpolation.

1. Introduction

The development of high order accurate, non-oscillatory shock capturing schemes currently is an area of active interest. High order accuracy is important for more complicated unsteady inviscid problems and for direct simulation of compressible flows. It is fairly straightforward to incorporate high order accuracy in non-conservative finite difference methods, however, shock capturing will not be possible. Finite volume methods and conservative finite difference methods, which retain this property, are unfortunately limited to first or second order accuracy in most cases. An important reason for this limitation in accuracy is the use of Total Variation Diminishing (TVD) methods to obtain non-oscillatory solutions. TVD methods are limited to first order accuracy in more than one dimension, Goodman and Leveque[3], and even in one dimension they reduce to first order accuracy at non-sonic local extrema, Osher and Chakravarthy[11].

Harten, Osher, Shu et al.[4,5,6,7,14,15] developed in recent years the so-called Essentially Non-Oscillatory (ENO) schemes, which do not have this limitation and have uniform high order accuracy outside discontinuities. In this paper the combination of the Osher approximate Riemann solver and the various ENO schemes for the solution of the Euler equations will be discussed. The discussion will be limited to one-dimensional problems, but important information for the development of multi-dimensional ENO methods can be obtained from the solution of several shock tube problems.

The main feature of ENO schemes is that they use an adaptive stencil. At each grid point a searching algorithm determines which part of the flow surrounding that grid point is the smoothest. This stencil is then used to construct a higher order accurate, conservative interpolation to determine the variables at the cell faces. This interpolation process can be applied to the conservative variables, characteristic variables or the fluxes, either defined as cell averaged or point values. The ENO scheme tries to minimize numerical oscillations around discontinuities by using predominantly data from the smooth parts of the flow field. Due to the constant stencil switching the ENO scheme is highly non-linear and only limited theoretical results are available, Harten and Osher[5] and Harten et al.[4].

†Present address, Member AIAA

An important subject in the ENO schemes is the numerical approximation of the fluxes at the cell faces. The Roe approximate Riemann solver is frequently used, while the Lax-Friedrichs flux splitting is preferred when the differentiability of the flux is important. The Roe scheme, however, requires a modification, because it does not satisfy the entropy condition and allows steady expansion shocks, whereas the Lax-Friedrichs scheme is very dissipative. When using an exact Riemann solver instead of the Roe approximation Harten et al.[6] obtained better results, while also the results of Shu and Osher[14,15] improved with a better flux approximation.

The Osher scheme, which is the most accurate approximate Riemann solver available, has some nice properties, which might improve the accuracy of ENO schemes. Until now the combination of the Osher and ENO scheme has not been investigated. Compared with the Roe approximate Riemann solver the Osher scheme is less popular due to the higher cost of computing the fluxes and the fact that it is more complicated than the Roe scheme. When using a higher order ENO scheme the cost of the Riemann solver, however, becomes less dominant, because the ENO interpolations themselves are quite expensive, especially for multi-dimensional problems. In addition a careful implementation of the Osher scheme does not have to be too expensive. The use of the Osher flux splitting has some additional benefits. It has a very low numerical dissipation in boundary layers compared to other Euler schemes, see for instance Koren[8]. Although beyond the scope of this paper this is an important consideration in the approximation of the inviscid contribution when solving the compressible Navier-Stokes equations for flows with both strong shocks and boundary layers by means of direct simulations. The possible application of ENO schemes in direct numerical simulations of compressible flow is the reason that the ENO schemes are tested up to fifth order accuracy.

As already mentioned there are various ways to construct ENO schemes. A good comparison of the different approaches unfortunately is lacking and will be part of this paper, with special emphasis on the combination of the Osher and ENO schemes. Several difficult shock tube cases are computed, which present a serious challenge to ENO schemes. In addition the effect of the ordering of the eigenvalues in the Osher scheme will be investigated, which is one of parameters which might effect the accuracy of the schemes. This comparison gives valuable information which of the approaches is the most successful. In the next section first a brief discussion of the Osher scheme for the Euler equations will be given. Next the construction of the various Osher-ENO schemes will be discussed and results of several shock tube tests will be given at the end of the paper.

2. Osher Scheme

The Osher-ENO scheme is used to solve the Euler equations of gas dynamics, which are defined as:

$$\mathbf{u}_t + \mathbf{f}(\mathbf{u})_x = 0 \qquad t > 0, -\infty < x < \infty \tag{2.1}$$

with initial data: $\mathbf{u}(x,0) = \mathbf{u}_0$. The vectors $\mathbf{u}$ and $\mathbf{f}$ are defined as $\mathbf{u} = (\rho, \rho u, e)^t$ and $\mathbf{f} = (\rho u, \rho u^2, (e+p)u)^t$. Here ρ, u, e and p represent the density, velocity, total energy and pressure respectively. The Jacobian matrix $\partial\mathbf{f}$ has real eigenvalues λ^i, $(\lambda^i = u-c, u, u+c)$, with c the speed of sound, and has a complete set of eigenvectors $\mathbf{r}^i$.

The system of equations (2.1) is completed with an equation of state for an ideal gas, $p = \rho RT$, with R the gas constant, and the relation between total energy and temperature, $T = e/(\rho c_v) - \frac{1}{2}u^2$, where c_v represents the specific heat at constant volume.

Let $\mathbf{u}_i^n = \mathbf{u}(x_i, t^n)$, $x_i = jh; t^n = n\tau$, with grid spacing h and time step τ, then the conservative first order approximation to the Euler equations can be written as:

$$\mathbf{u}_i^{n+1} = \mathbf{u}_i^n - \lambda(\mathbf{h}_{i+\frac{1}{2}} - \mathbf{h}_{i-\frac{1}{2}}) \tag{2.2}$$

with $\lambda = \tau/h$. The flux $\mathbf{h}$ at a cell face with index $i+\frac{1}{2}$ in the Osher scheme now is defined as:

$$\mathbf{h}_{i+\frac{1}{2}} = \frac{1}{2}(\mathbf{f}_i + \mathbf{f}_{i+1} - \int_{\Gamma_i} (\partial\mathbf{f}^+ - \partial\mathbf{f}^-)\, du) \tag{2.3}$$

with Γ_i a path in phase space. The matrices $\partial\mathbf{f}^\pm$ are defined as: $\partial\mathbf{f}^\pm = S\Lambda^\pm S^{-1}$, with S^{-1} the matrix with right eigenvectors $\mathbf{r}^i$ as columns, and
$\Lambda^+ = \mathrm{diag}(\max(0,\lambda^i))$; $\Lambda^- = \mathrm{diag}(\min(0,\lambda^i))$. Here diag is short for diagonal matrix. In the construction of the flux-ENO scheme we will also use the expression for the flux differences:

$$\mathbf{h}_{i+\frac{1}{2}} - \mathbf{h}_{i-\frac{1}{2}} = \int_{\Gamma_{i-1}} \partial\mathbf{f}^+ du + \int_{\Gamma_i} \partial\mathbf{f}^- du \tag{2.4}$$

By choosing a specific path in phase space, namely $\frac{du^i}{ds} = \mathbf{r}^i(s)$, Osher was able to derive explicit expressions for the integrals in equations (2.3-4) by separating the integrals along Γ^i into three parts. Along each path Γ_i one eigenvalue λ^i is constant and has a related set of Riemann invariants, $\lambda^{1,3} : \psi = \{u \pm \frac{2c}{\gamma-1}, \frac{p}{\rho^\gamma}\}$ and $\lambda^2 : \psi = \{u, p\}$. These Riemann invariants ψ are used to determine the intermediate states by linking them to $\mathbf{u}_i$ and $\mathbf{u}_{i+1}$, which are the end points of the path Γ_i. The order in which the eigenvalues are used in the

computation of the path integrals along Γ_i is important. The order $(u-c, u, u+c)$ is called the natural order, whereas $(u+c, u, u-c)$ is the reversed order. Osher and Solomon[9] were able to prove that the reversed order admits steady shocks in at most two points and satisfies the entropy condition, which guarantees convergence almost everywhere to the solution of the Euler equations in the limit $h \to 0$, $\tau \to 0$.

The integrals along each path can be computed using the fact that the eigenvalues are either genuinely nonlinear, $(\nabla_{\mathbf{u}}\lambda^i \cdot \mathbf{r}^i = 1)$, or linearly degenerate, $(\nabla_{\mathbf{u}}\lambda^i \cdot \mathbf{r}^i = 0)$. In the first case λ can have at most one zero on each path and in the second case it has no zeros. If there is a zero on a path, then the path integral has to be modified to treat the sonic point. The careful treatment of sonic points eliminates the possibility of expansion shocks which appear in the Roe method and also gives a differentiable flux vector.

The Osher scheme uses simple waves to solve the Riemann problem, which become multivalued in a shock. For an analysis of this phenomenon see Van Leer[16] and Dubois[2]. More details about the implementation of the Osher scheme and explicit expressions for the flux integrals can be found in Osher and Solomon[9], Chakravarthy and Osher [1] and Rai and Chakravarthy[13].

3. ENO Schemes

ENO schemes overcome the limitations of TVD schemes by relaxing the requirement of total variation non-increasing. They are conservative, essentially non-oscillatory and give uniform accuracy in smooth regions, without the degradation of accuracy at non-sonic local extrema as observed with TVD methods. There are several approaches possible when constructing ENO schemes. Harten, Osher, Engquist and Chakravarthy[6] use the ENO scheme to construct a higher order solution to the cell-average of equation (2.1) using a sliding average, defined as:

$$\overline{\mathbf{u}}(x,t) = \frac{1}{h}\int_{-\frac{h}{2}}^{\frac{h}{2}} \mathbf{u}(x+y,t)dy \qquad (3.1)$$

Integrating equation (2.1) over the domain $[x_{i-\frac{1}{2}}, x_{i+\frac{1}{2}}]$ gives:

$$\frac{\partial}{\partial t}\overline{\mathbf{u}}(x,t) + \frac{1}{h}[\mathbf{f}(\mathbf{u}(x+\frac{h}{2},t)) - \mathbf{f}(\mathbf{u}(x-\frac{h}{2},t))] = 0 \quad (3.2)$$

with grid spacing h. When considering this equation at the point $x = x_i$, the cell center, this gives the method of lines formulation for the cell average $\overline{\mathbf{u}}(x_i,t)$. Integrating in time finally gives the cell averaged equation:

$$\overline{\mathbf{u}}(x_i, t+\tau) = \overline{\mathbf{u}}(x_i,t) - \lambda[\mathbf{h}(x_{i+\frac{1}{2}}, t; \mathbf{u}) - \mathbf{h}(x_{i-\frac{1}{2}}, t; \mathbf{u})] \qquad (3.3)$$

with $\lambda = \tau/h$ and

$$\mathbf{h}(x,t;\mathbf{u}) = \frac{1}{\tau}\int_0^\tau \mathbf{f}(\mathbf{u}(x,t+\eta))d\eta \qquad (3.4)$$

The numerical flux in the ENO scheme from Harten et al. now is constructed such that it approximates the exact flux up to $O(h^r)$:

$$\overline{\mathbf{u}}_i^{n+1} - \left[\overline{E}_h(\tau)\cdot\overline{\mathbf{u}}^n\right]_i = O(h^r) \qquad (3.5)$$

with $\overline{E}_h(\tau)$ the numerical solution operator. The ENO scheme of Harten et al. therefore gives an r-th order accurate approximation to the cell averages. The most important ingredient of their ENO method is the reconstruction of the point values $\mathbf{u}(x)$ from the cell averaged values $\overline{\mathbf{u}}_i$. These point values are necessary to compute the flux $\mathbf{h}_{i+\frac{1}{2}}$ at the cell faces. This is done with a reconstruction method, discussed in the next section, such that the piecewise polynomial $R(x,\overline{\mathbf{u}})$ is conservative, viz. $\overline{R}(x_i,\overline{\mathbf{u}}) = \overline{\mathbf{u}}_i$, essentially non-oscillatory, $TV(R(\ \cdot\ ;\overline{\mathbf{u}})) \le TV(\overline{\mathbf{u}}) + O(h^r)$, and gives at all points in a neighborhood around x_i an r-th order approximation to $\mathbf{u}$, when $\mathbf{u}$ is smooth. The time integral, equation(3.4), then is computed using the Cauchy-Kowalewski procedure for hyperbolic systems and is discussed in the next section. This method has as benefit that it couples the spatial and temporal discretization.

In an alternative approach Shu and Osher[14,15] constructed the numerical solution directly from equation (3.2), with $x = x_i$, using a correction to the fluxes, obtained by a Taylor series expansion around the cell center x_i.

$$\hat{\mathbf{h}}_{i+\frac{1}{2}} = \mathbf{h}_{i+\frac{1}{2}} + \sum_{k=1}^{m-1} a_{2k} h^{2k} \left(\frac{\partial^{2k}\mathbf{h}}{\partial x^{2k}}\right)_{i+\frac{1}{2}} + O(h^{2m+1}) \qquad (3.6)$$

Here $\mathbf{h}_{i+\frac{1}{2}}$ is the flux obtained with any first order conservative scheme. The first few coefficients are: $a_2 = -\frac{1}{24}, a_4 = \frac{7}{5760}, \cdots$. This procedure makes the conservative formulation higher order accurate. This method is essentially a finite difference method and not a finite volume method, because $\overline{\mathbf{u}}(x_i,t)$ is now considered as a point value in the Taylor series expansion instead of a cell average. It is a generalization of the high resolution TVD schemes proposed by Osher and Chakravarthy[12].

In their second paper Shu and Osher[15] demonstrated that it is possible to construct a higher order method by reconstructing the fluxes directly from the fluxes computed from the cell averaged values without using this

formula. In this case the variable $\overline{\mathbf{u}}$ should be considered again as a cell averaged variable. This approach is used in section 3.2 for the flux-ENO method.
The time integration is performed using a new Runge-Kutta scheme which does not increase the total variation in time. This approach has as benefit that the spatial and temporal discretization are decoupled. This results in a simpler coding, but increased cost because the reconstruction, which is the most expensive part of the ENO schemes, has to be done at each stage of the Runge-Kutta scheme.

A hybrid approach is also possible, namely using the ENO scheme from Harten et al., but with the TVD Runge-Kutta method from Shu and Osher instead of the Cauchy-Kowalewski procedure for time integration. This method saves the cumbersome derivation of the higher derivatives of the solution but still does the ENO reconstruction on the primitive variables instead of the fluxes, which is generally more accurate. Results of this approach will be presented at the end of the paper.

The main benefit of the original point ENO method of Shu and Osher is that it is easy to extend to more dimensions using dimension splitting. Although in this way a higher order method, is obtained in practice it has a strong bias to the principle directions of the grid, which seriously degrades the accuracy. The approach of Harten et al. will give uniform higher order accuracy with a minimal grid dependence, but at significant cost and complexity, see Harten and Chakravarthy[7].

3.1 ENO-Osher scheme based on reconstruction from cell averaged variables

The implementation of the Osher scheme in the ENO method from Harten et al.[6], which uses a reconstruction from the cell averaged variables is straightforward. Only the Riemann solver has to be replaced with the Osher approximate Riemann solver, discussed in section 2. For completeness, however, a summary of this algorithm will be given. More details can be found in Harten et al.[6]. The first step in the ENO reconstruction is the determination of the primitive function $\mathbf{U}(x_{i+\frac{1}{2}})$ from the cell averaged variables:

$$\mathbf{U}(x_{i+\frac{1}{2}}) = \sum_{l=0}^{i} (x_{l+\frac{1}{2}} - x_{l-\frac{1}{2}})\overline{\mathbf{u}}_l \qquad (3.1.1)$$

A higher order polynomial representation of $\mathbf{U}$ in each cell is now constructed by determining the divided differences used in the Newton interpolation method using the following recursive algorithm: Start with $\mathbf{k}_{min} = i - \frac{1}{2}$ and $\mathbf{k}_{max} = i + \frac{1}{2}$, and the divided differences:

$$\mathbf{H}[x_{i-\frac{1}{2}}] \equiv \mathbf{U}(x_{i-\frac{1}{2}}); \quad \mathbf{H}[x_{i-\frac{1}{2}}, x_{i+\frac{1}{2}}] \qquad (3.1.2)$$

If the divided difference $\mathbf{H}[x_{i-\frac{3}{2}}, x_{i-\frac{1}{2}}, x_{i+\frac{1}{2}}]$ is larger than $\mathbf{H}[x_{i-\frac{1}{2}}, x_{i+\frac{1}{2}}, x_{i+\frac{3}{2}}]$ choose $\mathbf{H}[x_{i-\frac{1}{2}}, x_{i+\frac{1}{2}}, x_{i+\frac{3}{2}}]$ and $\mathbf{k}_{max} = x_{i+\frac{3}{2}}$; otherwise $\mathbf{H}[x_{i-\frac{3}{2}}, x_{i-\frac{1}{2}}, x_{i+\frac{1}{2}}]$ is accepted and $\mathbf{k}_{min} = x_{i-\frac{3}{2}}$. This process is repeated till the required order of the interpolation is obtained and applied to each component of $\mathbf{U}$ independently. It will give the interpolation of $\mathbf{U}$ and the stencil $[\mathbf{k}_{min}, \mathbf{k}_{max}]$. Here the divided differences are defined as:

$$\mathbf{H}[x_{i+\frac{1}{2}}, \cdots, x_{i+k+\frac{1}{2}}] = (\mathbf{H}[x_{i+\frac{3}{2}}, \cdots, x_{i+k+\frac{1}{2}}] - \mathbf{H}[x_{i+\frac{1}{2}}, \cdots, x_{i+k-\frac{1}{2}}])/(x_{i+k+\frac{1}{2}} - x_{i+\frac{1}{2}}) \qquad (3.1.3)$$

After the determination of the coefficients of the Newton polynomial it is straightforward to obtain the point values by differentiation of the Newton interpolation polynomial, because $\mathbf{u} = \frac{\partial}{\partial x}\mathbf{U}$. This process is greatly simplified using the algorithm discussed in the Appendix in Harten et al.[6], which transforms the Newton polynomial representation into a series expansion around x_i:

$$R(x;\overline{\mathbf{u}}) = \sum_{k=0}^{r-1} \mathbf{b}_{i,k}(x - x_i)^k \qquad (3.1.4)$$

This process gives a representation of the solution in each cell and can be used to determine the values of $\mathbf{u}$ at the cell faces $x_{i\pm\frac{1}{2}}$. The values at the left and right side of the cell are now used in the Osher approximate Riemann solver, which gives the fluxes $\mathbf{f}_{i\pm\frac{1}{2}}$. This reconstruction process can be applied directly to the conservative variables, but in order to minimize the interactions between the different equations it is preferable first to transform $\overline{\mathbf{u}}$ to characteristic variables and transform back after the reconstruction.

The method of lines approach can now be followed, solving equation (3.2), with the TVD Runge-Kutta method, or the Cauchy-Kowalewski procedure can be used to solve equation (3.3). The TVD Runge-Kutta method is an r-th order, $\bar{r}$ stage Runge-Kutta method defined as:

$$\mathbf{u}^{(i)} = \sum_{k=0}^{i-1} \left[\alpha_{ik}\mathbf{u}^{(k)} + \beta_{ik}\tau L(\mathbf{u}^{(k)})\right], \quad i = 1, \cdots \bar{r} \qquad (3.1.5)$$

with

$$\mathbf{u}^{(0)} = \mathbf{u}^n, \quad \mathbf{u}^{(\bar{r})} = \mathbf{u}^{n+1} \qquad (3.1.6)$$

Here L represents the spatial discretization operator. For the coefficients α, β see Shu and Osher[14]. The TVD Runge-Kutta method has as main benefit that it

does not increase the total variation during the time integration step.

The alternative is to use equation (3.3) and compute the integral, equation (3.4). This integral is discretized by means of a Gaussian quadrature formula:

$$\int_0^\tau \mathbf{f}(\mathbf{u}(x_{i+\frac{1}{2}}, t+\eta))d\eta = \sum_{k=0}^{K} \alpha_k \mathbf{f}\left(\mathbf{u}(x_{i+\frac{1}{2}}, \beta_k \tau)\right) + O(\tau^r) \tag{3.1.7}$$

The values of $\mathbf{u}(x_{i+\frac{1}{2}}, \beta_k\tau)$ are now determined using the Cauchy-Kowalewski procedure, which is essentially a Taylor series expansion around the point (x_i, t^n):

$$\mathbf{u}(x,t) = \sum_{l=0}^{r-1}\sum_{k=0}^{l} \frac{\partial^l \mathbf{u}(x_i,t^n)}{\partial x^k \partial t^{l-k}} \frac{(x-x_i)^k}{k!} \frac{t^{l-k}}{(l-k)!} \tag{3.1.8}$$

The derivatives $\frac{\partial^l \mathbf{u}(x_i,t^n)}{\partial x^k \partial t^{l-k}}$ can be obtained by differentiation of the original differential equation (2.1) and using the coefficients $\mathbf{b}_{il}$ which are equal to $\frac{\partial^l \mathbf{u}}{\partial x^l}$.

$$\frac{\partial \mathbf{u}(x_i,t^n)}{\partial x^l} = \mathbf{b}_{il}; \qquad 0 \le l \le r-1 \tag{3.1.9}$$

3.2 Osher flux-ENO method

The Osher flux-ENO method is constructed using the flux difference relation for the Osher scheme, equation (2.4). The ENO reconstruction is applied directly to the fluxes in a conservative way, as proposed by Shu and Osher[15]. The reconstruction is, however, more complicated due to the path integrals in the Osher flux, equation (2.3). Define the flux $\mathbf{f}$ in a cell centered around x_i as $\mathbf{f} = \int_{x_{i-\frac{1}{2}}}^{x_{i+\frac{1}{2}}} \mathbf{g}(\xi)$ then $\mathbf{f}$ satisfies the relation

$$\mathbf{f}(\mathbf{u}_i) = \mathbf{F}(x_{i+\frac{1}{2}}) - \mathbf{F}(x_{i-\frac{1}{2}}))/h \tag{3.2.1}$$

with the primitive function $\mathbf{F}$ defined as:
$\mathbf{F}(x) = \int_\infty^x \mathbf{g}(\xi)d\xi$. The conservative flux difference for a cell with index i then can be determined directly from the primitive function $\mathbf{F}$, which is determined with the ENO reconstruction technique. The flux-ENO reconstruction is now applied directly to the positive and negative fluxes in the Osher scheme, defined as:

$$\mathbf{df}^{\pm}_{i+\frac{1}{2}} = \int_{\Gamma_i} \partial \mathbf{f}^{\pm} du \tag{3.2.2}$$

These relations, cannot be used directly because the primitive functions $\mathbf{F}^{\pm}$ are not known, nor the fluxes $\mathbf{f}^{\pm}$ themselves. Their explicit form, however, is not needed, only their divided differences which can be linked to $\mathbf{df}^{\pm}$ by means of the following relations:

$$\begin{aligned}\mathbf{df}^{+}_{i+\frac{1}{2}} &= \mathbf{f}^{+}_{i} - \mathbf{f}^{+}_{i-1} \\ &= \mathbf{F}^{+}[x_{i+\frac{1}{2}}, x_{i-\frac{1}{2}}] - \mathbf{F}^{+}[x_{i-\frac{1}{2}}, x_{i-\frac{3}{2}}] \\ &= (x_{i+\frac{1}{2}} - x_{i-\frac{3}{2}})\mathbf{F}^{+}[x_{i+\frac{1}{2}}, x_{i-\frac{1}{2}}, x_{i-\frac{3}{2}}]\end{aligned} \tag{3.2.3}$$

with an equivalent relation for $\mathbf{df}^{-}_{i+\frac{1}{2}}$:

$$\begin{aligned}\mathbf{df}^{-}_{i+\frac{1}{2}} &= \mathbf{f}^{-}_{i+1} - \mathbf{f}^{-}_{i} \\ &= \mathbf{F}^{-}[x_{i+\frac{3}{2}}, x_{i+\frac{1}{2}}] - \mathbf{F}^{-}[x_{i+\frac{1}{2}}, x_{i-\frac{1}{2}}] \\ &= (x_{i+\frac{3}{2}} - x_{i-\frac{1}{2}})\mathbf{F}^{-}[x_{i+\frac{3}{2}}, x_{i+\frac{1}{2}}, x_{i-\frac{1}{2}}]\end{aligned} \tag{3.2.4}$$

Here $\mathbf{F}^{\pm}[x_0, \cdots, x_k]$ represent the k-th divided differences of $\mathbf{F}^{\pm}$. These relations automatically introduce upwinding for the positive and negative wave directions. Higher order approximations can be obtained by extending the divided difference tables of $\mathbf{F}^{\pm}$, using the following recursive algorithm for the positive flux, which is slightly different from the one discussed in section 3.1.

Start with $\mathbf{k}_{min} = i$. If the divided difference
$F^{+}_{k}[x_{k^{(l-1)}_{min}-\frac{1}{2}}, \cdots, x_{k^{(l-1)}_{min}+l-\frac{1}{2}}]$ is larger than
$F^{+}_{k}[x_{k^{(l-1)}_{min}-\frac{3}{2}}, \cdots, x_{k^{(l-1)}_{min}+l-\frac{3}{2}}]$ choose
$F^{+}_{k}[x_{k^{(l-1)}_{min}-\frac{3}{2}}, \cdots, x_{k^{(l-1)}_{min}+l-\frac{3}{2}}]$ and $k_{min} = k_{min} - 1$
else $F^{+}_{k}[x_{k^{(l-1)}_{min}-\frac{1}{2}}, \cdots, x_{k^{(l-1)}_{min}+l-\frac{1}{2}}]$ is accepted and k_{min} remains unchanged. This process is done for all the components k of the flux vector $\mathbf{f}^{+}$ during each interpolation step l and continued up to the required order. The following Newton polynomial now can be constructed:

$$P^{(l)}_{k}(x) = P^{(l-1)}_{k}(x) + c^{(l)}_{k} \prod_{i=k^{(l-1)}_{min}}^{k^{(l-1)+l-1}_{min}} (x - x_{i-\frac{1}{2}}) \tag{3.2.5}$$

where $c^{(l)}_{k}$ is the divided difference accepted in the l-th interpolation step. A similar algorithm is used for the negative fluxes $\mathbf{f}^{-}$ with $\mathbf{k}_{min} = i$, replaced by $\mathbf{k}_{min} = i+1$. Here $\mathbf{k}_{min}$ is the left most stencil of the grid centered around point i; whereas $P^{(l)}_{k}$ represents the l-th order Newton interpolation polynomial. The index k refers to the application of the ENO reconstruction to each component of the flux vectors $\mathbf{f}^{\pm}$ independently. This algorithm automatically chooses the smoothest possible interpolation stencil: $\{\mathbf{k}^{\pm}_{min}, \cdots, \mathbf{k}^{\pm}_{min} + l - 1\}$, independently for each component of the positive and negative fluxes. By continuously comparing the divided differences, obtained by adding one point to the left and one to the right, it is decided which one gives the

smoothest interpolation. Adding the positive and negative fluxes, and using the relation for the flux difference for the Osher scheme, equation (2.4), now gives the flux difference for the cell with index i:

$$\mathbf{h}_{i+\frac{1}{2}} - \mathbf{h}_{i-\frac{1}{2}} = \frac{d}{dx}\mathbf{P}^{-}_{i+\frac{1}{2}}|_{x=x_{i+\frac{1}{2}}} + \frac{d}{dx}\mathbf{P}^{+}_{i-\frac{1}{2}}|_{x=x_{i-\frac{1}{2}}} \tag{3.2.6}$$

The time integration is accomplished using the TVD Runge-Kutta scheme of Shu and Osher[14], discussed in the previous section.

The use of the relations

$$\mathbf{df}^{+}_{i+\frac{1}{2}} = \mathbf{f}_{i+1} - \mathbf{h}_{i+\frac{1}{2}} \tag{3.2.6}$$

$$\mathbf{df}^{-}_{i+\frac{1}{2}} = \mathbf{h}_{i+\frac{1}{2}} - \mathbf{f}_{i}$$

to obtain the positive and negative fluxes, as suggested by Shu and Osher[14], without presenting an application in their paper, does not give a higher order scheme. The reason is that this relation is based on the average of a forward and backward flux, which is only a second order accurate approximation to $\mathbf{h}_{i+\frac{1}{2}}$. In order to obtain higher order accuracy this average will have to be replaced by a higher order interpolation, which would require an additional reconstruction step.

4. Discussion and Results

To test the combination of the different ENO schemes and the Osher scheme several shock tube calculations were performed. The cases were chosen to test the schemes for the various types of discontinuities which exist as solutions of the Euler equations, viz. shocks, contact discontinuities and expansion waves. The initial conditions were kindly provided by F. Coquel and are summarized in Table 1. They were designed to be severe tests for shock capturing schemes and are helpful in detecting possible flaws in the different ENO schemes. For all cases the three possible ENO schemes, viz. ENO with primitive variable reconstruction, with either the Cauchy-Kowalewski procedure for time integration (ENO-CK) or the TVD Runge-Kutta method (ENO-RK), or the reconstruction applied directly to the fluxes (ENO-FL), were tested. The number of grid points was 162 and maximum CFL number .8. In some cases the CFL number had to be reduced due to numerical instabilities, namely case B with ENO-RK and case E with ENO-CK required a CFL number .1 for 4th and 5th order accuracy, whereas for all schemes the maximum CFL number had to be reduced to .6 for 5th order accuracy. All methods were tested with spatial accuracy ranging from first order up to fifth order. The time accuracy was always equal to the spatial accuracy for ENO-CK. For ENO-RK and ENO-FL the time accuracy was limited to third order. The TVD Runge-Kutta scheme becomes rather awkward for fourth and higher order accuracy. It has a strong CFL limitation, requires a large amount

	P_L	U_L	T_L	P_R	U_R	T_R
	$[N/m^2]$	$[m/sec]$	$[K]$	$[N/m^2]$	$[m/sec]$	$[K]$
A	15000	0	1378	98400	0	4390
B	988000	0	2438	9930	0	2452
C	10000	0	2627	100000	0	272
E	573	2200	199	22300	0	546

Table 1. Initial conditions shock tube cases

of temporary storage and is not practically useful. In addition to testing the various ENO schemes also the effect of the ordering of the eigenvalues in the Osher scheme has been investigated. For code validation purposes several of the cases presented by Harten et al.[6], such as Sod's problem were computed and compared well with their results.

The first case, labeled A in Table 1., consists of a left moving shock, followed by a contact discontinuity and a right moving expansion wave. In all the plots the continuous line is the exact solution while the lines with dots and triangles represent the numerical results. The vertical axis of one curve was shifted upwards to make the differences between the various methods more clear. All plots, except Fig. 9, show the results using the reversed ordering of eigenvalues in the Osher scheme. In Fig. 1-3 results of the various methods for 2nd and 5th order accuracy are presented for the density profile. The density is the critical variable in this problem, because of the contact discontinuity. This means that points in the region between shock and contact discontinuity have a discontinuity in both directions, which is the worst possible case for an ENO scheme, because in both directions the reconstruction will always have to cross a discontinuity for third or higher order reconstructions. Due to the extremely low dissipation of the higher order schemes these numerical oscillations, created in the initial stages when there are not enough points in the region between the two discontinuities to build a higher order non-oscillatory reconstruction, will remain in the solution. It is clear that ENO-CK is superior in this region, while ENO-RK still gives a reasonable result, although the method is slightly more dissipative than ENO-CK and has a small overshoot. The ENO-FL reconstruction, however, has strong oscillations for third and higher order in the region between

the shock and contact discontinuity. Pressure and velocity are monotone for all schemes and different orders of accuracy. All methods represent the region behind the contact discontinuity and the expansion wave equally well and no major differences exist between the reversed or natural ordering of the eigenvalues in the Osher scheme. It should be borne in mind that due to the fact that the solution of the Riemann problem is self similar only first order accuracy is possible and the shock tube tests merely show that solutions with higher order methods can be obtained without numerical oscillations. Test of all methods on free convection problems, however, showed that all methods reached the proper order of accuracy. Higher order methods, especially ENO-CK, however, still give a better solution than first order methods for flows with discontinuities. Especially the smearing in the region between the shock and contact discontinuity reduces.

The second test, case B, is different from case A in that it has a sonic point in the expansion wave. The first order solution therefore has an $O(\triangle x)$ expansion wave at the sonic point, but does not need an entropy fix as does the Roe method. This discontinuity is stronger for the natural order than for the reversed order of eigenvalues in the Osher scheme. The disturbance is about twice as large for the natural order and although greatly reduced for higher order methods it consistently slightly reduces the accuracy in this area, when using the natural order. This is a general conclusion for all cases with a sonic point. Both ENO-CK and ENO-FL work reasonably well, with ENO-CK, with reversed order of eigenvalues, superior, as can be seen in Fig. 4-5. The flux-ENO method experiences a small jump around the sonic point due to the limited differentiability of the Osher flux at this point. This problem would require additional attention when using the flux-ENO method to obtain uniform high order solutions, but for the comparison of different ENO methods it is not relevant. The ENO-RK method experienced serious oscillations at the beginning and end of the expansion wave, Fig. 6, and was unstable for fifth order accuracy, when using the natural ordering. Both natural and reversed order became oscillatory, but the natural order turned out to be more sensitive in general. In cases of instability the differences, however, were not large enough to prefer one method for the other. The other two methods also experience small problems at the bottom of the expansion wave, but much less severe. A clear explanation for this phenomenon still is lacking and will require further research.

The third problem, case C, has as main feature a strong contact discontinuity. The different

Order	ENO-FL	ENO-CK	ENO-RK
2	1.	1.13	2.15
3	1.70	1.73	3.68
4	1.91	2.07	4.15
5	2.13	3.12	4.62

Table 2. Comparison CPU time of different ENO schemes

schemes behave similar in the region with the expansion wave as in case B, with the reversed order slightly better around the sonic point. All methods experience a small undershoot in the region between the contact discontinuity and the expansion wave, with ENO-CK, Fig. 7, the most accurate and ENO-FL has some high frequency oscillations, see Fig. 8. The smearing of the contact discontinuity is approximately equal for all methods, but slightly reduces with higher order accuracy. Contrary to case B, ENO-RK now does not experience instability problems.

The final test, case E, which consists of two strong shocks moving in opposite directions is the most difficult case. The first order Osher scheme with natural ordering of eigenvalues is not monotone and has a significant overshoot in density, pressure and velocity at the first point behind the left moving shock, Fig. 9. The Osher scheme with reversed ordering is monotone. All ENO schemes are already oscillatory for second order accuracy. The second order ENO-CK scheme, with reversed ordering of eigenvalues experiences some small oscillations in the pressure behind the shock, Fig. 11, but the density still is nearly monotone, Fig. 10. The reason for the oscillations are the same as those discussed for case A. In the initial stages there are not enough points between the two shocks to build a non-oscillatory reconstruction. This phenomenon is, however, stronger for case E than for case A, because this problem only occurred in case A for the density which had a region separated by a shock and contact discontinuity, but not for the other variables. When a region is separated by two shocks also the pressure and velocity are discontinuous. Contrary to the expectations the second order flux-ENO method, which was oscillatory for case A now is nearly monotone. All ENO schemes are oscillatory for third and higher order, as can be seen in Fig. 12-13.

The choice between the different ENO methods is not only determined by its accuracy but also by its numerical efficiency. Table 2. shows the relative CPU time for the different methods. The flux-ENO method is the least expensive, but the ENO-CK scheme is nearly equal up to 4-th order. The difference at 5-th order

is caused by the fact that the other two schemes only use the third order accurate TVD Runge-Kutta scheme, while ENO-CK also is fifth order accurate in time. Table 2 also shows that the ENO-RK scheme is significantly more expensive and requires approximately twice as much CPU time.

5. Conclusions

In all cases the ENO-CK method, with reversed ordering of eigenvalues in the Osher scheme, was superior or performed equally well as the other ENO schemes and is the most robust. The ordering of eigenvalues in the Osher scheme is not extremely critical. The natural ordering, however, has a larger jump around a sonic point, which slightly reduces the accuracy of higher order approximations. The natural ordering also experiences a slightly larger level of numerical oscillations than the reversed ordering. In cases were the first order scheme with natural ordering is not monotone it is not possible to build higher order non-oscillatory schemes. This stresses the importance of a good approximate Riemann solver.

The ENO method, with TVD Runge-Kutta time integration, is more dissipative and less robust than the ENO method with the Cauchy-Kowalewski procedure for time integration. Although it requires a significant effort to derive all the higher order derivatives for a multi-dimensional problem, it certainly pays off when one considers the fact that the TVD Runge-Kutta method requires multiple reconstructions, which are the most expensive part of the algorithm, and significant larger storage. The flux-ENO method, although having the benefit of being the most easy to program, and fairly straightforward to extend to multiple dimensions does not have the robustness of the primitive variable reconstruction.

Acknowledgments

The author would like to express his gratitude for many helpful discussions with Prof. J. Ferziger, Stanford University, and Drs. F. Coquel, ONERA, and A. Suresh, Sverdrup Technology.

References

1. Chakravarthy, S.R. and Osher, S, "Numerical Experiments with Osher Upwind Scheme for the Euler Equations", *AIAA Journal*, Vol. 21, 1983, pp. 1241-1248.
2. Dubois, F., "Boundary Conditions and the Osher Scheme for the Euler Equations of Gas Dynamics", Ecole Polytechnique, Centre de Mathématiques Appliquées, Report 150, Palaiseau, France, 1987.
3. Goodman, J. and LeVeque, R., On the Accuracy of Stable Schemes for 2D Scalar Conservation Laws", *Mathematics of Computation*, Vol. 45, 1985, pp. 15-21.
4. Harten, A., Osher, S., Engquist, B. and Chakravarthy, S.R., "Some Results on Uniformly High Order Accurate Essentially Non-Oscillatory Schemes", *Journal of Applied Numerical Mathematics*, Vol. 2, 1986, pp. 347-377.
5. Harten, A. and Osher, S., "Uniformly High-Order Accurate Nonoscillatory Schemes I", *SIAM Journal on Numerical Analysis*, Vol. 24, 1987, pp. 279-309.
6. Harten, A., Engquist, B., Osher, S. and Chakravarthy, S.R., "Uniformly High Order Accurate Essentially Non-Oscillatory Schemes III", *Journal of Computational Physics*, Vol. 71, 1987, pp. 231-303.
7. Harten, A. and Chakravarthy, S.R., "Multi-Dimensional ENO Schemes for General Geometries", ICASE Report 91-76, NASA Langley, Virginia, 1991.
8. Koren, H., "Upwind Discretization of the Steady Navier-Stokes Equations", *International Journal for Numerical Methods in Fluids*, Vol. 11, 1990, pp. 99-117.
9. Osher, S. and Solomon, F., "Upwind Difference Schemes for Hyperbolic Systems of Conservation Laws", *Mathematics of Computation*, Vol. 38,1982, pp. 339-374.
10. Osher, S. and Chakravarthy, S.R., "Upwind Schemes and Boundary Conditions with Applications to Euler Equations in General Geometries", *Journal of Computational Physics*, Vol. 50, 1983, pp. 447-481.
11. Osher, S. and Chakravarthy, S.R., "High Resolution Schemes and the Entropy Condition", *SIAM Journal on Numerical Analysis*, Vol. 21, 1984, pp. 955- 984.
12. Osher, S. and Chakravarthy, S.R., "Very High Order TVD Schemes", *Mathematics and its Applications*, Vol. 2, 1986, pp. 229-274.
13. Rai, M.M. and Chakravarthy, S.R., "An Implicit Form for the Osher Upwind Scheme", *AIAA Journal*, Vol. 24, 1986, pp. 735-743.
14. Shu, C.-W. and Osher, S., "Efficient Implementation of Essentially Non-Oscillatory Shock-Capturing Schemes", *Journal of Computational Physics*, Vol. 77, 1988, pp. 439-471.
15. Shu, C.-W. and Osher, S., "Efficient Implementation of Essentially Non-Oscillatory Shock Capturing Schemes, II", *Journal of Computational Physics*, Vol. 83, 1989, pp. 32-78.
16. Van Leer, B., "On the Relation Between the Upwind-Differencing Schemes of Godunov, Engquist-Osher and Roe", *SIAM Journal on Sci. Stat. Comput.*, **5**, 1984, pp. 1-20.

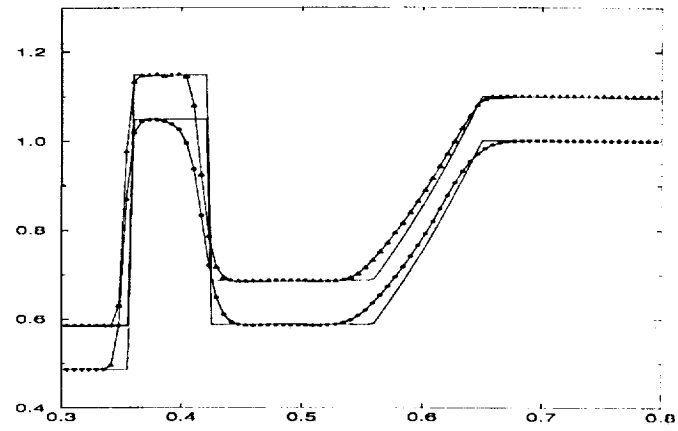

Figure 1. Case A, density at $t = .2$, 2nd (dots) and 5th order (triangles) ENO-CK.

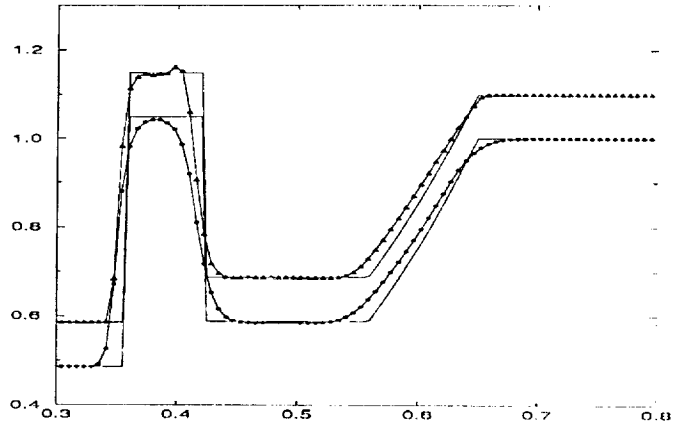

Figure 2. Case A, density at $t = .2$, 2nd (dots) and 5th order (triangles) ENO-RK.

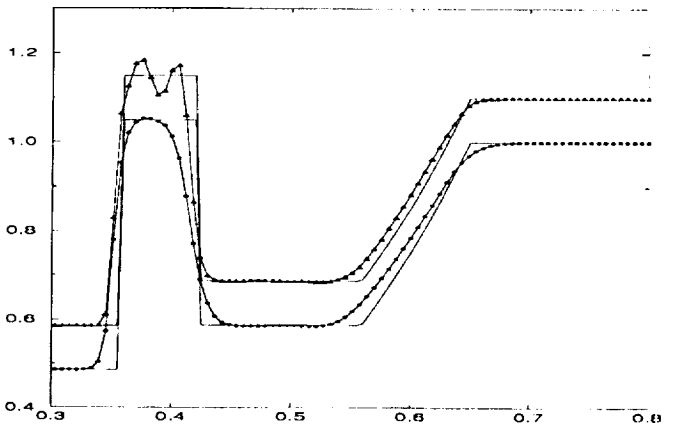

Figure 3. Case A, density at $t = .2$, 2nd (dots) and 5th order (triangles) ENO-FL.

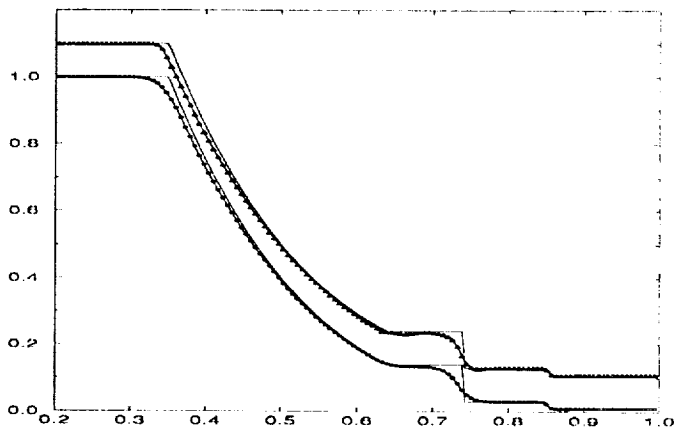

Figure 4. Case B, density at $t = .2$, 2nd (dots) and 5th order (triangles) ENO-CK.

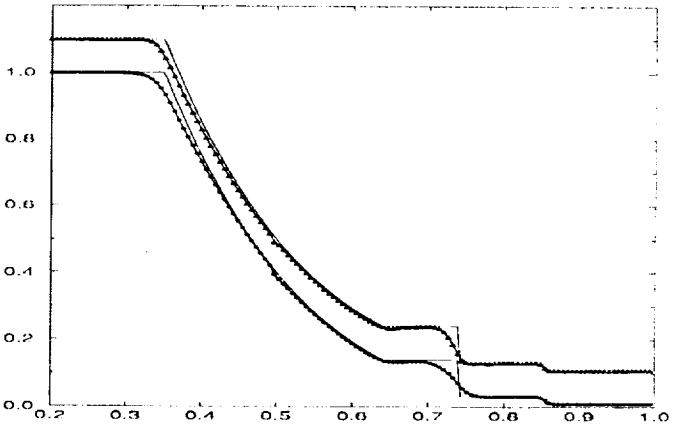

Figure 5. Case B, density at $t = .2$, 2nd (dots) and 5th order (triangles) ENO-FL.

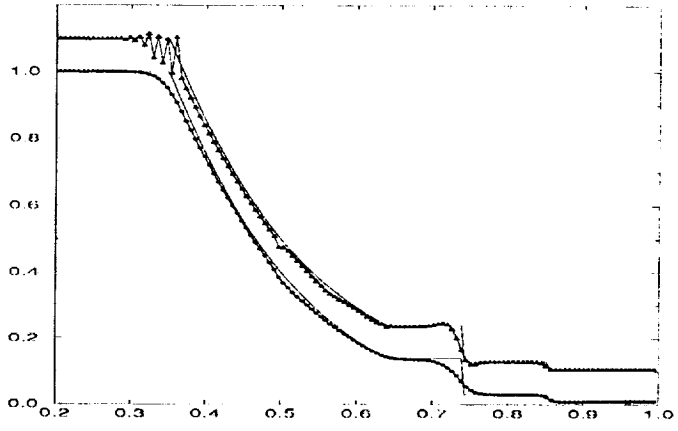

Figure 6. Case B, density at $t = .2$, 2nd (dots) and 5th order (triangles) ENO-RK.

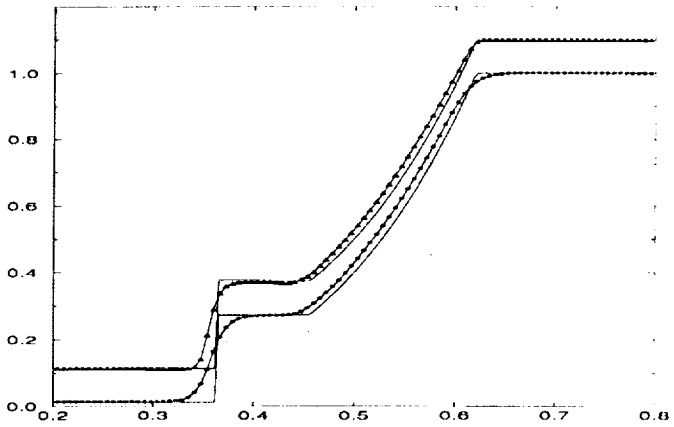

Figure 7. Case C, density at $t = .5$, 2nd (dots) and 5th order (triangles) ENO-CK.

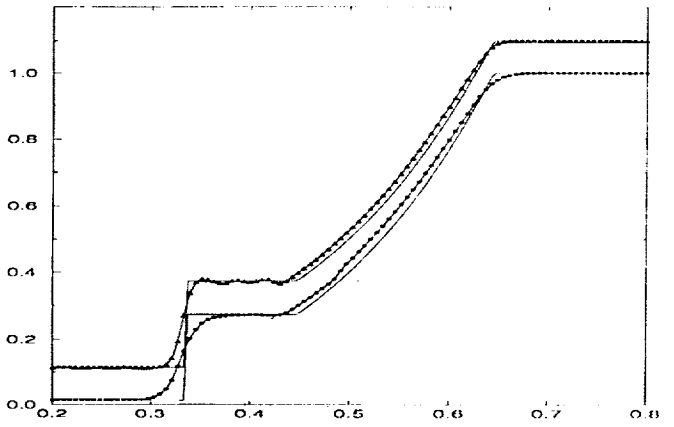

Figure 8. Case C, density at $t = .5$, 2nd (dots) and 5th order (triangles) ENO-FL.

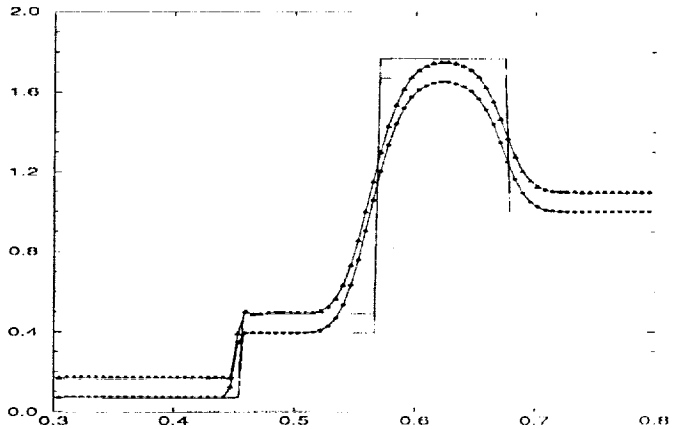

Figure 9. Case E, density at $t = .6$, 1st order Osher scheme, natural (triangles) and reversed order (dots).

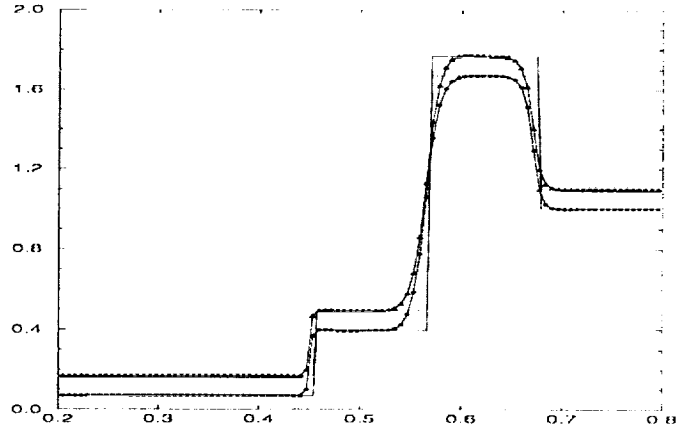

Figure 10. Case E, density at $t = .6$, 2nd order ENO-CK (dots) and ENO-FL (triangles).

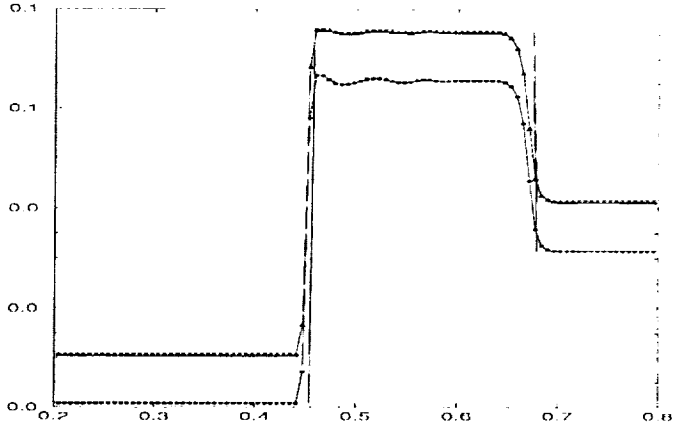

Figure 11. Case E, pressure at $t = .6$, 2nd order ENO-CK (dots) and ENO-FL (triangles).

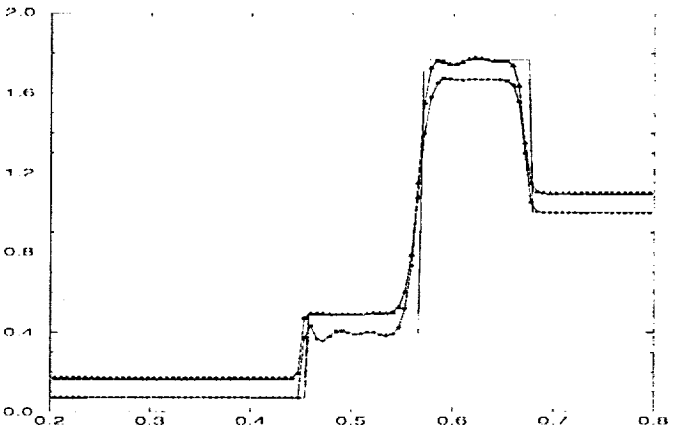

Figure 12. Case E, density at $t = .6$, 3nd order ENO-CK (dots) and ENO-FL (triangles).

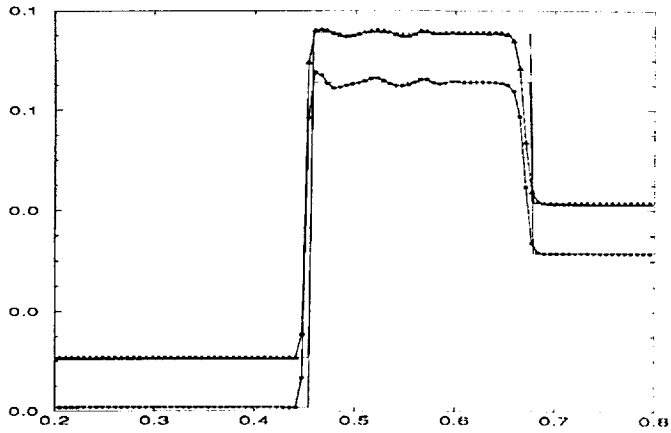

Figure 13. Case E, pressure at $t = .6$, 3nd order ENO-CK (dots) and ENO-FL (triangles).

REPORT DOCUMENTATION PAGE

Form Approved
OMB No. 0704-0188

1. AGENCY USE ONLY (*Leave blank*)	2. REPORT DATE	3. REPORT TYPE AND DATES COVERED
	November 1992	Technical Memorandum

4. TITLE AND SUBTITLE

Eno-Osher Schemes for Euler Equations

5. FUNDING NUMBERS

WU-505-62-21

6. AUTHOR(S)

Jacobus J. Van Der Vegt

7. PERFORMING ORGANIZATION NAME(S) AND ADDRESS(ES)

National Aeronautics and Space Administration
Lewis Research Center
Cleveland, Ohio 44135-3191

8. PERFORMING ORGANIZATION REPORT NUMBER

E-7435

9. SPONSORING/MONITORING AGENCY NAMES(S) AND ADDRESS(ES)

National Aeronautics and Space Administration
Washington, D.C. 20546-0001

10. SPONSORING/MONITORING AGENCY REPORT NUMBER

NASA TM-105928
ICOMP-92-21
CMOTT-92-10

11. SUPPLEMENTARY NOTES

Prepared for the 31st Aerospace Science Meeting and Exhibit sponsored by the American Institute of Aeronautics and Astronautics, Reno, Nevada, January 11-14, 1993 (AIAA-93-0335). Jacobus J. Van Der Vegt, Institute for Computational Mechanics in Propulsion, Lewis Research Center (work funded under Space Act Agreement C99066G) and Center for Turbulence Research, Stanford University, Building 500, Stanford, California 94305. Space Act Monitor: Louis A. Povinelli.

12a. DISTRIBUTION/AVAILABILITY STATEMENT

Unclassified - Unlimited
Subject Category 64

12b. DISTRIBUTION CODE

13. ABSTRACT ***(Maximum 200 words)***

In this paper the combination of the Osher approximate Riemann solver for the Euler equations and various ENO schemes is discussed for one-dimensional flow. The three basic approaches, viz. the ENO scheme using primitive variable reconstruction, either with the Cauchy-Kowalewski procedure for time integration or the TVD Runge-Kutta scheme, and the flux-ENO method are tested on different shock tube cases. The shock tube cases were chosen to present a serious challenge to the ENO schemes in order to test their ability to capture flow discontinuities, such as shocks. Also the effect of the ordering of the eigen values, viz. natural or reversed ordering, in the Osher scheme is investigated. The ENO schemes are tested up to fifth order accuracy in space and time. The ENO-Osher scheme using the Cauchy-Kowalewski procedure for time integration is found to be the most accurate and robust compared with the other methods and is also computationally efficient. The tests showed that the ENO schemes perform reasonably well, but have problems in cases where two discontinuities are close together. In that case there are not enough points in the smooth part of the flow to create a non-oscillatory interpolation.

14. SUBJECT TERMS

Euler equations; Eno schemes

15. NUMBER OF PAGES

12

16. PRICE CODE

A03

17. SECURITY CLASSIFICATION OF REPORT	18. SECURITY CLASSIFICATION OF THIS PAGE	19. SECURITY CLASSIFICATION OF ABSTRACT	20. LIMITATION OF ABSTRACT
Unclassified	Unclassified	Unclassified	